Report on the Effects of the Use of a Non-Zero B-angle and Interpolation in the Generation of Leakage Matrices on MPTS Frequencies, Widths, and Asymmetries

A) Effects of the Use of a Non-Zero B-angle

In this report, we will compare the frequencies, line widths, and line asymmetries from the following two tables of fitted mode parameters: HMI.100430to0710b-6.354.v0 and HMI.100430to0710.v7. Both tables were generated with the MPTS method and are based on the same 72-day observing run of the HMI that ran from April 30 through July 10 of 2010. For the generation of the "v7" table, the reference set of leaks corresponding to a B-angle of zero were used, while for the generation of the "v0" table leaks corresponding to a B-angle of -6.354 degrees were used. The leaks for the B-angle of -6.354 degrees were kindly generated by Dr. Larson. In Table 1 we have listed the averages and standard deviations of both the raw and normalized differences of the frequencies, line widths, and line asymmetries. We have also included the absolute magnitude of the t-values and the probabilities that the sample differences occurred by chance are listed in the columns labeled $|t|$ and p, respectively. For the remainder of this report, we will refer to this case of using different B-angles in the generation of the two sets of leakage matrices as the "Bang" case.

difference		raw				normalized			
mode parameter	$n_{\rm d}$	ave	std	$\lvert t\rvert$	p	ave	std	$\lvert t\rvert$	p
ν	7329	$+0.0021$	0.0810	2.265	0.024	$+0.0892$	0.5265	14.499	≈ 0
w	7329	-0.0029	0.1619	1.538	0.124	-0.0151	0.1044	12.357	≈ 0
B	7329	$+0.0000$	0.0061	0.152	0.879	-0.0147	0.0622	20.253	≈ 0

Table 1: Averages and standard deviations of both the raw and normalized differences of the frequencies, ν, line widths, w, and line asymmetries, B, that were obtained from the table of fitted mode parameters HMI.100430to0710b-6.354.v0 and HMI.100430to0710.v7, respectively. All types of differences were computed in the sense HMI.100430to0710.v7 minus HMI.100430to0710b-6.354.v0. The normalizaton was carried out by dividing the raw differences by the formal error of each difference. Using Student's t-Test, each mean raw and each mean normalized frequency difference was tested for a significant deviation from zero. The absolute magnitude of the t-value and the probability that the sample difference occurred by chance are listed in the columns labeled $|t|$ and p, respectively. The reason we are showing $|t|$ is because we are employing a one-sided hypothesis test (i.e., $H_0:$ ave $= 0$). Since we are using a one-sided test, it is irrelevant whether ave < 0 or ave > 0. In the column labeled $n_{\rm d}$ the number of data points are given. The raw differences of both the frequencies and line widths are measured in μHz.

The probabilities given in column 6 of Table 1 show that at the 2.5 % significance level we can reject the null hypothesis that the average raw frequency differences was equal to 0, while we can accept the null hypothesis for both the average of the raw width differences and the average of the raw asymmetry differences. The probabilities given in the tenth column of Table 1 show that we can reject the null hypothesis for the normalized frequency, width, and asymmetry differences.

We show the raw frequency differences for the Bang case as a function of the spherical harmonic degree in the upper-left panel of Figure 1 and we show the same raw frequency differences as a function of frequency in the upper-right panel of the same figure. Both of these panels are dominated

by the outliers that are the largest at low degrees and high frequencies, so any systematic differences are obscured at the y-axis scale that is used in both panels.

We show the normalized frequency differences for the Bang case as a function of the spherical harmonic degree in the lower-left panel of Figure 1 and we show the same raw frequency differences as a function of frequency in the lower-left panel of the same figure. The lower-left panel shows a positive bump for degrees centered around $l = 250$ and an apparent decrease with increasing degrees above $l = 350$. The lower-right panel shows both large positive and negative outliers at frequencies below $\nu = 1500\,\mu$Hz, which are caused by the rather small errors of the frequency differences that can be seen at low frequencies in Figure 3. For frequencies between 1500 and $2500\,\mu$Hz the normalized frequency differences appear to get larger with increasing frequency before they begin to go through a minimum around $3200\,\mu$Hz.

Because the presence of the large outlying raw frequency differences in both of the upper panels of Figure 1 obscured the presence of any possible systematic differences, we binned them as functions of both degree and frequency. The binned raw frequency differences are shown in the upper-left panel of Figure 2 and they are shown as a function of frequency in the upper-right panel. The upper-left panel shows a large peak for the bin centered at $l = 250$ followed by a nearly monotonic decrease with increasing degree above this bin. Only a dip centered at $l = 450$ and a peak centered at $l = 1050$ deviate from this downward trend in the binned raw frequency differences. The upper-right panel shows random differences for frequencies below $1750\,\mu$Hz followed by a peak that is centered around a frequency of $2500\,\mu$Hz. The error bars in all four panels are the standard errors of the mean values within each bin.

The binned normalized frequency differences for the Bang case are shown in the two lower panels of Figure 2. The similarity in the shapes of the curves in the two left-hand panels is obvious as is the similarity in the shapes of the curves in the two right-hand panels. Taken together, all four panels of Figure 2 suggest the major effect of the use of the non-zero B-angle on the frequencies is to cause a decrease in the frequencies of the p1, p2, and p3 ridges centered on the $l = 250$, $\nu = 2500\,\mu$Hz region of the dispersion plane. (Even though the panels in Figure 2 show an increase for this region, since the subtractions were carried out in the sense ofHMI.100430to0710.v7 minus HMI.100430to0710b-6.354.v0, this bump actually corresponds to smaller frequencies in theHMI.100430to0710b-6.354.v0 file than in the HMI.100430to0710.v7 file.)

In the first row of Table 2, we show the number of bins for which the error bars did not cross zero and the total number of bins. We show that when the binning was done as a function of degree 64 % of the error bars did not cross zero and when the binning was done as a function of frequencies 75 % of the error bars did not cross zero. In the second row of this table, we show the similar statistics for the normalized frequency differences. For these differences the percentage of the degree bins for which the error bars did not include zero was 64 % for the degree bin and 69 % for the frequency bins. These four percentages are all large enough to indicate that at the level of one standard error of the mean, both the binned raw and binned normalized frequency differences for the Bang case showed systematic differences from zero. In particular, the degree distribution of the bins whose error bars do not cross zero supports the idea that the most significant feature in the two left-hand panels of Figure 2 is the large bump that is centered on $l = 250$. Similarly, the frequency distribution of the bins whose error bars do not cross zero supports the idea that the most significant feature in the two right-hand panels of Figure 2 is the bump centered on the frequency of $2500\,\mu$Hz.

The base-10 logarithms of the formal errors, $\sigma_{\Delta\nu}$, of the raw frequency differences are shown as a function of the frequency in Figure 3. This figure shows the presence of very small errors for a few of the p-mode ridges at low frequencies followed by a broad plateau for $2000 \leq \nu \leq 3250\,\mu$Hz, which in turn is followed by a systematic increase for higher frequencies.

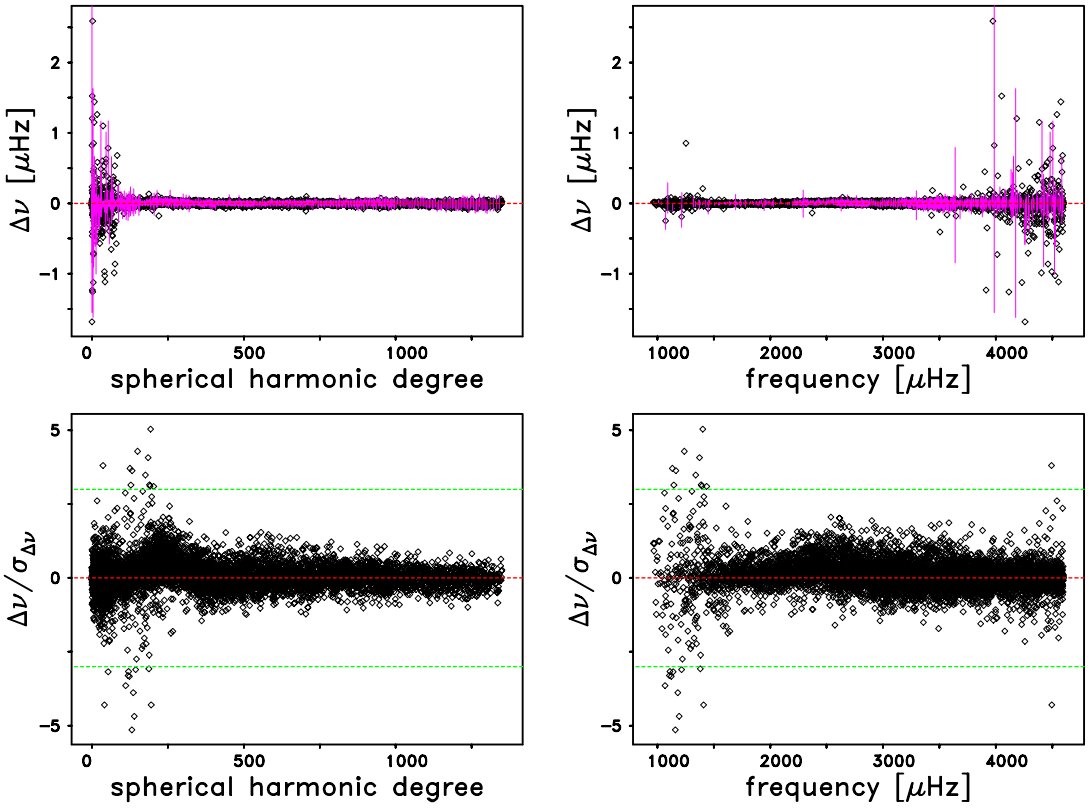

Figure 1: (Upper-left panel) Frequency differences $\Delta\nu = \nu_{\rm HMI.100430to0710.v7} - \nu_{\rm HMI.100430to0710b-6.354.v0}$ as functions of the spherical harmonic degree for the ridges $n = 0$ through $n = 30$. For some selected differences the error bar is shown in magenta. The error bars are the square root of the sum of the squares of the uncertainties of the two sets of frequencies. The dashed red line is for a difference of zero. (Upper-right panel) Same as upper-left panel, but for the frequency differences $\Delta\nu$ as functions of the frequency. (Bottom-left panel) Same as upper-left panel, but for the normalized frequency differences. The normalization was carried out by dividing the raw frequency differences, $\Delta\nu$, as shown in the upper left-hand panel, by the formal error, $\sigma_{\Delta\nu}$, of each difference. The dashed green lines show the $\pm 3\sigma$ values. (Bottom-right panel) Same as bottom-left panel, but for the normalized frequency differences as functions of the frequency.

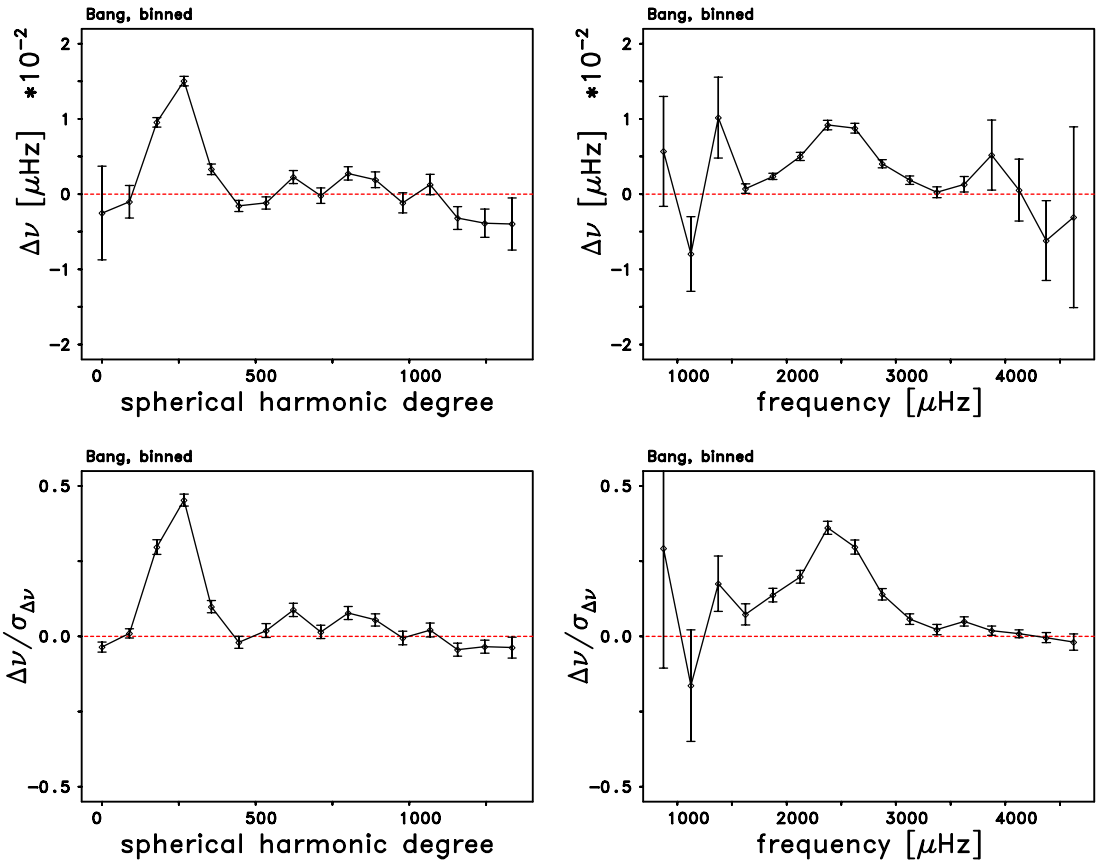

Figure 2: (Upper-left panel) Binned raw frequency differences $\Delta\nu = \nu_{\rm HMI.100430to0710.v7} - \nu_{\rm HMI.100430to0710b-6.354.v0}$ versus spherical harmonic degree using 100-degree wide bins. (Upper-right panel) Same as upper-left panel, except that the binned raw frequency differences are plotted versus frequency using 250 μHz-wide bins. (Bottom-left panel) Same as upper-left panel, except that the binned normalized frequency differences are shown. The normalization was carried out by dividing the raw frequency differences $\Delta\nu$ by the formal error of each difference. (Bottom-right panel) Same as bottom-left panel, except that the binned normalized frequency differences are plotted versus frequency. In all four panels the error bars are the standard errors of the means, and the dashed red line is for a difference of zero.

differences	# degree bins where the error bar does not cross zero	# frequency bins where the error bar does not cross zero
raw	9 of 14	12 of 16
normalized	9 of 14	11 of 16

Table 2: Number of degree and frequency bins, respectively, where the error bar does not cross zero for the comparison of the binned raw and normalized frequency differences $\Delta\nu = \nu_{\rm HMI.100430to0710.v7} - \nu_{\rm HMI.100430to0710b-6.354.v0}$.

In Figure 4 we show both the raw and the normalized differences $w_{\rm HMI.100430to0710.v7} - w_{\rm HMI.100430to0710b-6.354.v0}$ of the line widths both as functions of the spherical harmonic degree and of the frequency. As can be seen in both of the upper panels, aside from three outliers the raw differences of the line widths are smaller than $\pm 2.5\,\mu$Hz. Aside from the same three outlying points,

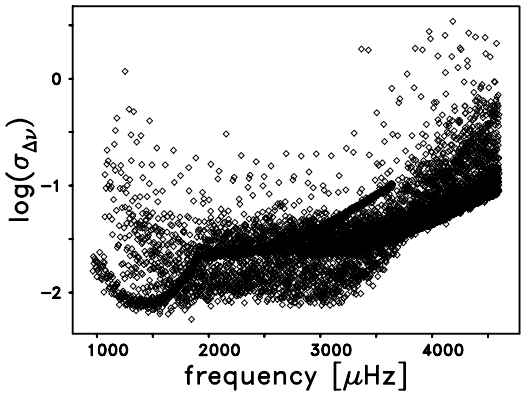

Figure 3: Frequency dependence of the logarithm of the formal errors, $\sigma_{\Delta\nu}$, of the frequency differences, $\Delta\nu$, as shown in the top panels of Figure 1.

the normalized differences of the line widths, $\Delta w/\sigma_{\Delta w}$, as shown in the two lower panels, do not exceed the $\pm 0.8\,\sigma$ level. Looking at both of the lower panels, we can see that the normalized width differences are negative for a region of the l-ν plane centered around $l = 300$ and $\nu = 3200\,\mu$Hz, and they are positive for a second region centered around $l = 400$ and $\nu = 2000\,\mu$Hz. Apart from these two groups of modes, the remainder of the normalized width differences are all close to zero.

Because the presence of the large outlying raw line width differences in both of the upper panels of Figure 4 obscured the presence of any possible systematic differences, we binned them as functions of both degree and frequency. The binned raw line width differences are shown in the left-hand panel of Figure 5 and they are shown as a function of frequency in the right-hand panel. The left-hand panel shows a broad dip for the bin centered at $l = 350$ followed by a monotonic increase which crosses through zero around $l = 700$ and continues to a global maximum at $l = 1350$. The right-hand panel shows a broad peak centered around $\nu = 1750\,\mu$Hz followed by a very broad dip that is centered around a frequency of $3500\,\mu$Hz. The error bars in both panels are the standard errors of the mean values within each bin. In the left-hand panel we can see that, when the binning was done as a function of degree, 88 % of the error bars do not cross zero, while in the right-hand panel, when the binning was done as a function of frequency, 81 % of the error bars do not cross zero. These two percentages are large enough to indicate that at the level of one standard error of the mean, both sets of binned raw line width differences for the Bang case showed systematic differences from zero. Taken together, the two panels of Figure 5 suggest that the effect of the non-zero B-angle was to increase the line widths of modes having degrees between 250 and 650 and frequencies above $2300\,\mu$Hz. (While the two panels of Figure 5 show dips in the line widths for this group of modes, the sense of the subtractions means that the line widths were larger in the HMI.100430to0710.v7 minus HMI.100430to0710b-6.354.v0 file than they were in the HMI.100430to0710.v7 file.)

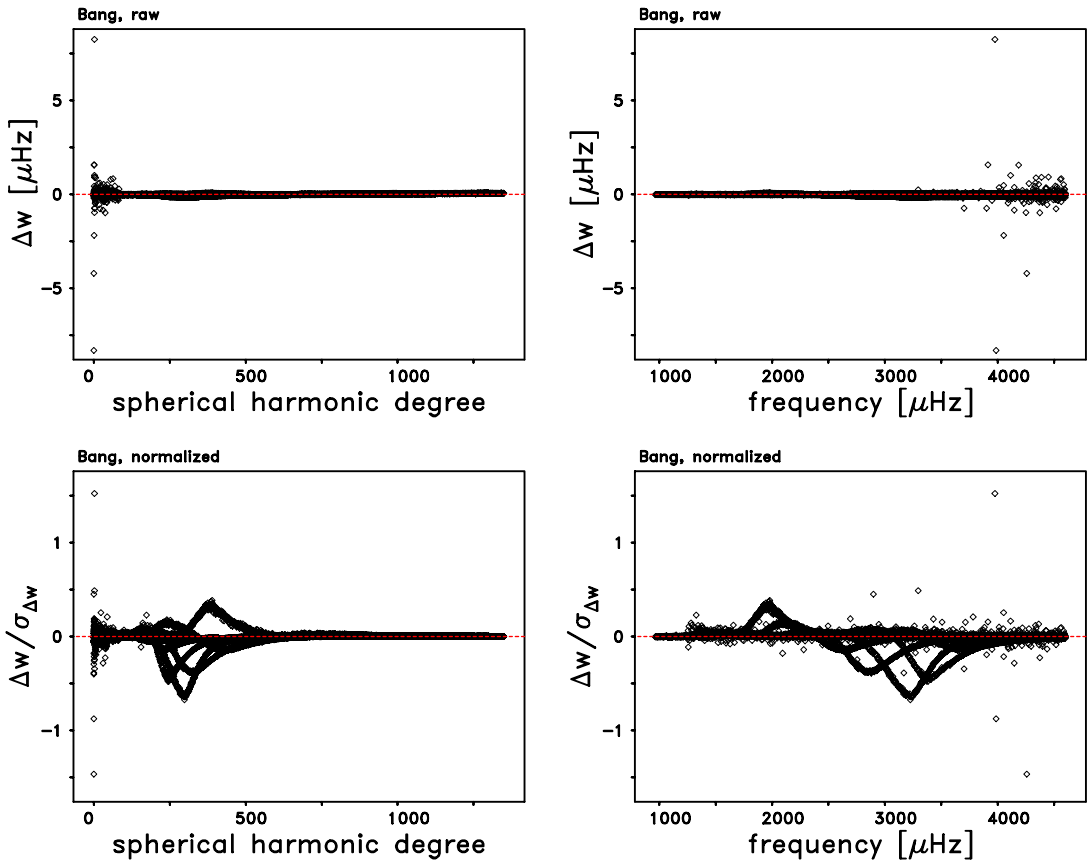

Figure 4: (Upper-left panel) Line width differences $\Delta w = w_{\mathrm{HMI.100430to0710.v7}} - w_{\mathrm{HMI.100430to0710b-6.354.v0}}$ as functions of the spherical harmonic degree for the ridges $n = 0$ through $n = 30$. The dashed red line is for a difference of zero. (Upper-right panel) Same as upper-left panel, but for the line width differences Δw as functions of the frequency. (Bottom-left panel) Same as upper-left panel, but for the normalized line width differences. The normalization was carried out by dividing the raw line width differences, Δw, as shown in the upper left-hand panel, by the formal error, $\sigma_{\Delta w}$, of each difference. (Bottom-right panel) Same as bottom-left panel, but for the normalized line width differences as functions of the frequency.

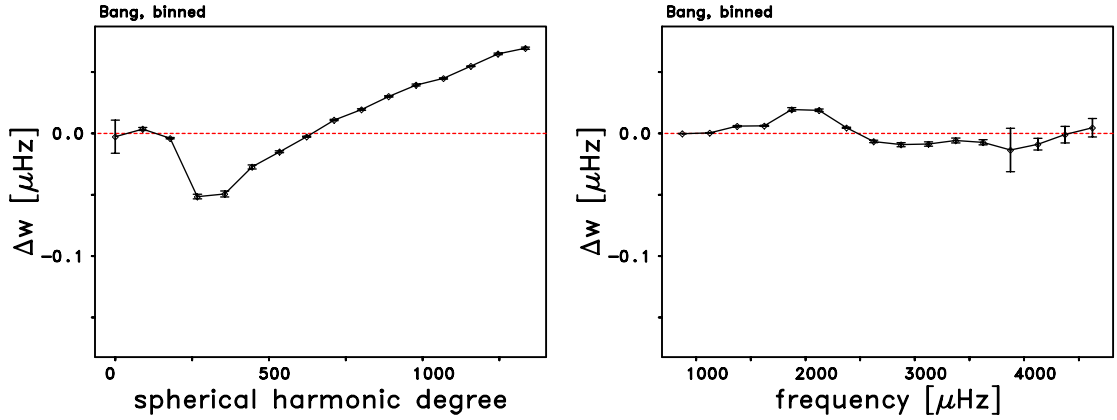

Figure 5: (Left panel) Binned line width differences $\Delta w = w_{\mathrm{HMI.100430to0710.v7}} - w_{\mathrm{HMI.100430to0710b-6.354.v0}}$ as functions of the spherical harmonic degree for the ridges $n = 0$ through $n = 30$. The dashed red line is for a difference of zero. (Right panel) Same as left-hand panel, but for the binned line width differences Δw as functions of the frequency.

In Figure 6 we show both the raw and the normalized differences $B_{\mathrm{HMI.100430to0710.v7}} - B_{\mathrm{HMI.100430to0710b-6.354.v0}}$ of the line asymmetries as functions of the spherical harmonic degree. Appreciable raw differences of the line asymmetries only occur for $l < 250$; and, with the exception of three outliers, all of those differences are less than $\pm 0.1\,\mu$Hz. Apart from three outliers, the normalized differences in the line asymmetries, $\Delta B/\sigma_{\Delta B}$, are in the range $\pm 0.3\,\sigma$. These normalized differences do show a broad negative bulge centered around $l = 250$.

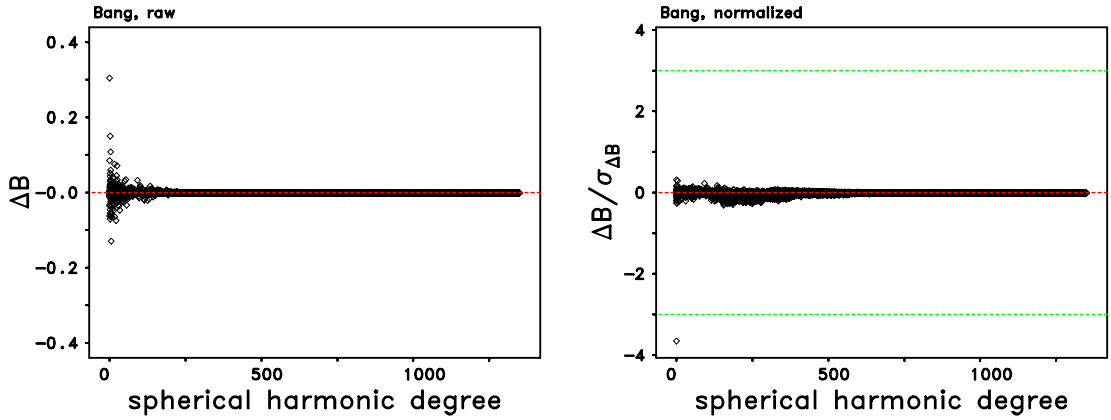

Figure 6: (Left panel) Line asymmetry differences $\Delta B = B_{\mathrm{HMI.100430to0710.v7}} - B_{\mathrm{HMI.100430to0710b-6.354.v0}}$ as functions of the spherical harmonic degree for the ridges $n = 0$ through $n = 30$. The dashed red line is for a difference of zero. (Right panel) Same as left panel, but for the normalized line asymmetry differences. The normalization was carried out by dividing the raw line asymmetry differences, ΔB, as shown in the left-hand panel, by the formal error, $\sigma_{\Delta B}$, of each difference. The dashed green lines show the $\pm 3\sigma$ values.

We show the binned raw line asymmetry values in Figure 7. They are shown as a function of degree in the left-hand panel and as a function of frequency in the right-hand panel. The left-hand panel shows that below $l = 300$ the error bars on all three of the bins include zero, so those differences appear to be random. Beginning with a dip centered at $l = 290$, the remaining binned values monotonically approach zero with increasing degree. On the other hand, the right-hand panel shows there is no significant trend in the binned asymmetries as function of frequency.

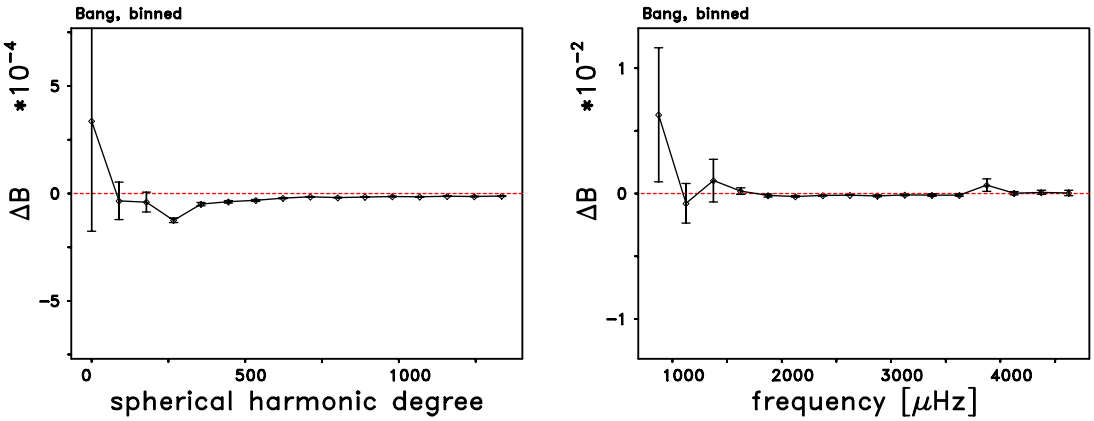

Figure 7: (Left panel) Binned line asymmetry differences $\Delta B = B_{\mathrm{HMI.100430to0710.v7}} - b_{\mathrm{HMI.100430to0710b-6.354.v0}}$ as functions of the spherical harmonic degree for the ridges $n = 0$ through $n = 30$. The dashed red line is for a difference of zero. (Right panel) Same as left-hand panel, but for the binned line asymmetry differences ΔB as functions of the frequency.

B) Effects of Interpolation on Modal Parameters

In this section, we compare the frequencies, line widths, and line asymmetries that came from the same HMI.100430to0710.v7 table that was employed in Section A) above with the corresponding parameters that came from a third table of mode parameters that we named HMI.100430to0710.i.v0, respectively. While for the generation of the "v7" table the complete set of reference leaks which corresponded to the B-angle of zero were used, for the generation of the "i.v0" table an interpolated version of the same reference set of leaks was used instead. The interpolated table of the referece set of leaks was kindly generated by Dr. Tim Larson. For the remainder of this report, we will refer the case of interpolated leakage matrices as the "iplkm" case. Each set of differences was computed in the sense HMI.100430to0710.i.v0 minus HMI.100430to0710.v7. Hence, it is important to note that the sense of the subtractions for the iplkm case was opposite the sense of the subtractions for the Bang case.

In Table 3 we list the averages and standard deviations of both the raw and normalized differences of the frequencies, line widths, and line asymmetries. We list also the absolute magnitude of the t-values and the probabilities that the sample differences occurred by chance in the columns labeled $|t|$ and p, respectively. Because the sense of the subtractions in the iplkm comparisons was opposite the sense of the subtractions in the Bang comparisons that we showed in Section A) above, we need to mentally reverse all six of the signs of the differences in Table 3. After reversing these signs, we note that all six of the raw and normalized average differences had the same signs in both the Bang and iplkm comparisons. These sign changes will also need to be kept in mind when comparing Figures 1 and 2 and Figures 4 through 7 with Figures 8 through 13.

difference		raw				normalized			
mode parameter	$n_{\rm d}$	ave	std	$\lvert t\rvert$	p	ave	std	$\lvert t\rvert$	p
ν	7327	-0.0020	0.0693	2.510	0.012	-0.0497	0.3683	11.538	≈ 0
w	7327	-0.0163	0.1757	7.927	≈ 0	-0.0094	0.0402	20.023	≈ 0
B	7327	-0.0000	0.0070	0.586	0.558	$+0.0037$	0.0524	6.012	≈ 0

Table 3: Averages and standard deviations of both the raw and normalized differences of the frequencies, ν, line widths, w, and line asymmetries, B, as obtained from the tables of fitted mode parameters HMI.100430to0710.i.v0 and HMI.100430to0710.v7, respectively. All types of differences were computed in the sense HMI.100430to0710.i.v0 minus HMI.100430to0710.v7. The normalizaton was carried out by dividing the raw differences by the formal error of each difference. Using Student's t-Test, each mean raw and each mean normalized frequency difference was tested for a significant deviation from zero. The absolute magnitude of the t-value and the probability that the sample difference occurred by chance are listed in the columns labeled $|t|$ and p, respectively. The reason we are showing $|t|$ is because we are employing a one-sided hypothesis test (i.e., $H_0:$ ave $= 0$). Since we are using a one-sided test, it is irrelevant whether ave < 0 or ave > 0. In the column labeled $n_{\rm d}$ the number of data points are given. The raw differences of both the frequencies and line widths are measured in μHz. In the column labeled $n_{\rm d}$ the number of data points are given. The raw differences of both the frequencies and line widths are measured in μHz.

Comparison of the first rows of Tables 1 and 3 shows that the overall averages of the two sets of raw frequency differences were nearly identical in magnitude. Comparison of the p values in column 6 of the same row of both tables shows that we can reject the null hypothesis for the two raw averages at the 2.5 % significance level. Furthermore, while the overall average of the normalized Bang frequency differences was 79 % larger than the overall average of the iplkm

frequency differences, comparison of the p values in column 10 of the first row of both tables shows that we can reject the null hypothesis for both sets of the normalized frequency differences.

Comparison of the second rows of Tables 1 and 3 shows that even though the overall average of the raw iplkm line width differences was 5.6 times larger than the average of the raw Bang line widths, the two p values in the sixth column of this row show that we can reject the null hypothesis for both sets of line width differences at the 2.5 % significance level. Similarly, even though the average of the normalized Bang line width differences was equal to 1.62 times the average of the normalized iplkm line width differences, the two p values in the tenth column of this row show that the null hypothesis can be rejected for both sets of line width differences.

Comparison of the third rows of Tables 1 and 3 shows that the average differences of both sets of raw asymmetry differences were equal to zero to four significant figures. Comparison of the p values in column 6 of this row show that we cannot reject the null hypothesis for both sets of the raw asymmetries. Also, while the average of the normalized Bang asymmetry differences was equal to four times the average of the normalized iplkm asymmetry differences, the two p values in the tenth column of this row show that we can reject the null hypothesis for both sets of the normalized asymmetry differences.

In Figure 8 we show both the raw and the normalized differences $\nu_{\mathrm{HMI.100430to0710.i.v0}} - \nu_{\mathrm{HMI.100430to0710.v7}}$ both as functions of the spherical harmonic degree and of the frequency. As was the case with the two upper panels in Figure 1, the two upper panels of Figure 8 are dominated by the presence of the outliers which are located at low degrees and high frequencies. Because the presence of these outliers makes it impossible to see the existence of any trends in these differences, we have also shown the normalized iplkm frequency differences in the two lower panels of Figure 8. The lower-left panel of Figure 8 indicates that the normalized frequency differences were negative for degrees above about $l = 500$. The lower-right panel of Figure 8 indicates that the majority of the normalized frequency differences for frequencies above 2250 μHz were also negative.

We show the binned iplkm raw frequency differences in the two upper panels of Figure 9 and we show the binned iplkm normalized frequency differences in the two lower panels. Taken together, all four panels of Figure 9 show that the main effect of the use of interpolation in the leakage matrices was a decrease in the frequencies of the f, p1, p2, and p3 ridges for degrees above $\ell = 450$.

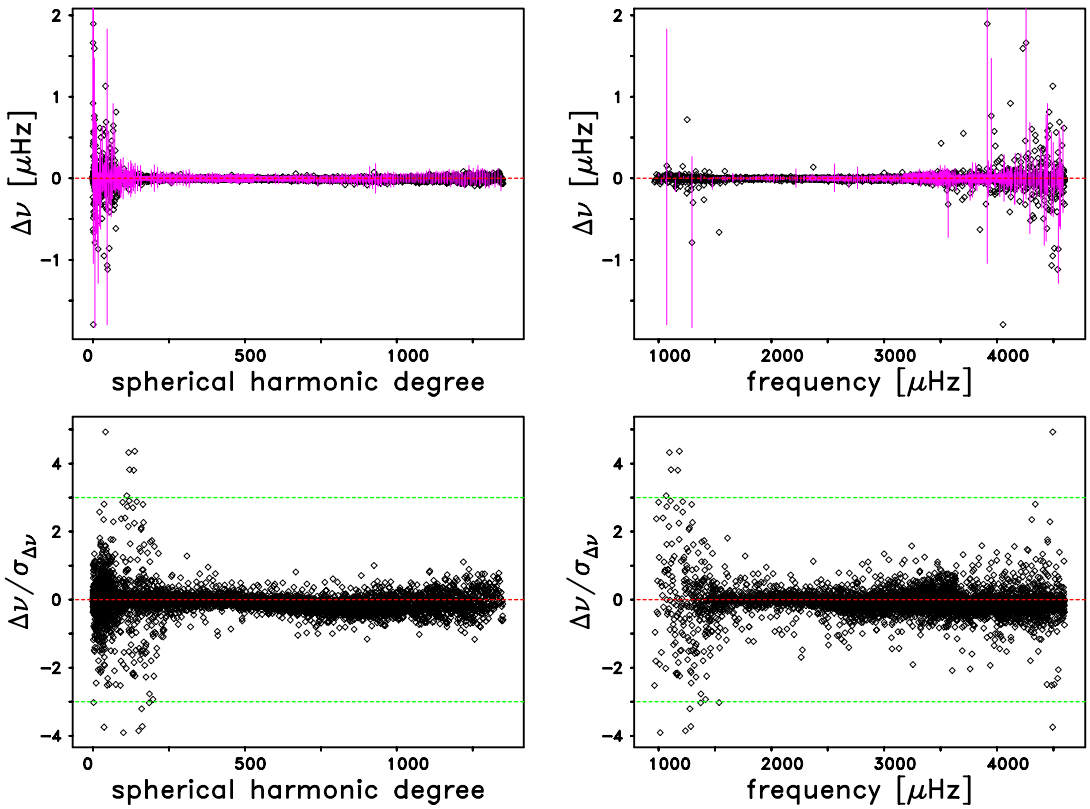

Figure 8: (Upper-left panel) Frequency differences $\Delta\nu = \nu_{\rm HMI.100430to0710.i.v0} - \nu_{\rm HMI.100430to0710.v7}$ as functions of the spherical harmonic degree for the ridges $n = 0$ through $n = 30$. For some selected differences the error bar is shown in magenta. The error bars are the square root of the sum of the squares of the uncertainties of the two sets of frequencies. The dashed red line is for a difference of zero. (Upper-right panel) Same as upper-left panel, but for the frequency differences $\Delta\nu$ as functions of the frequency. (Bottom-left panel) Same as upper-left panel, but for the normalized frequency differences. The normalization was carried out by dividing the raw frequency differences, $\Delta\nu$, as shown in the upper left-hand panel, by the formal error, $\sigma_{\Delta\nu}$, of each difference. The dashed green lines show the $\pm 3\,\sigma$ values. (Bottom-right panel) Same as bottom-left panel, but for the normalized frequency differences as functions of the frequency.

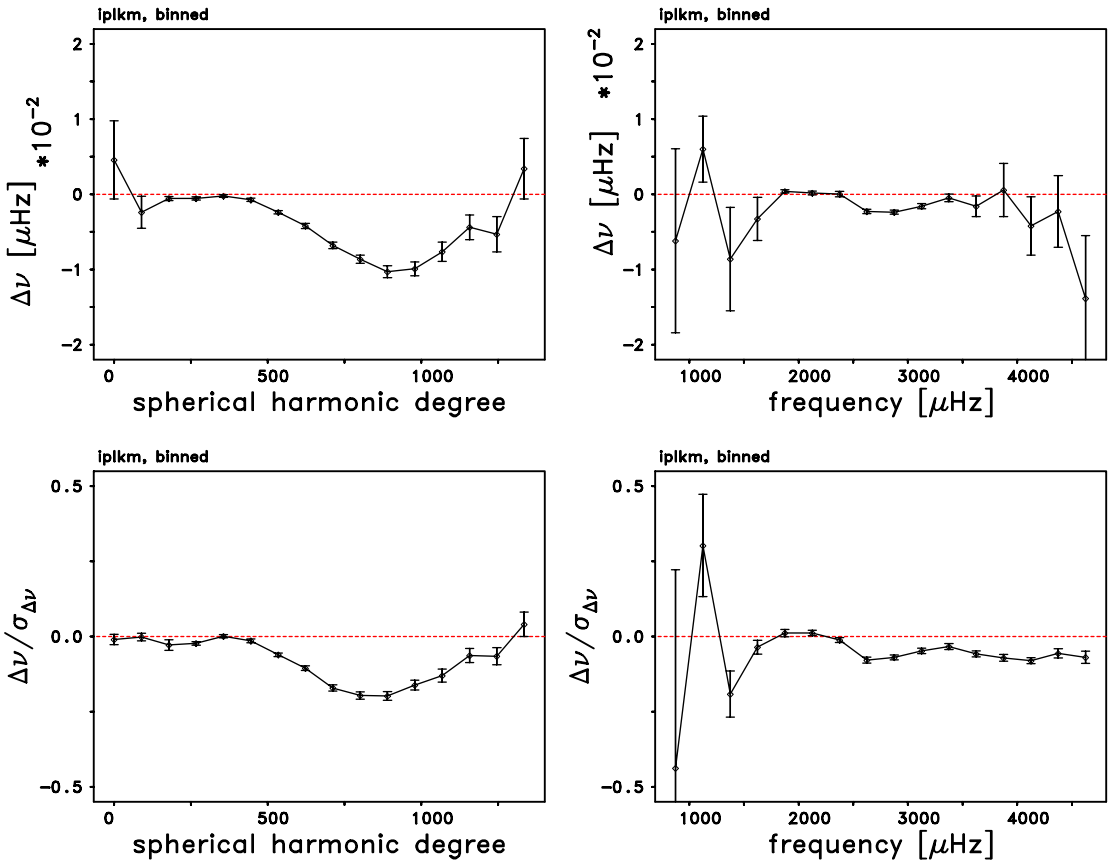

Figure 9: (Upper-left panel) Binned raw frequency differences $\Delta\nu = \nu_{\rm HMI.100430to0710.i.v0} - \nu_{\rm HMI.100430to0710.v7}$ versus spherical harmonic degree using 100-degree wide bins. (Upper-right panel) Same as upper-left panel, except that the binned raw frequency differences are plotted versus frequency using 250 μHz-wide bins. (Bottom-left panel) Same as upper-left panel, except that the binned normalized frequency differences are shown. The normalization was carried out by dividing the raw frequency differences $\Delta\nu$ by the formal error of each difference. (Bottom-right panel) Same as bottom-left panel, except that the binned normalized frequency differences are plotted versus frequency. In all four panels the error bars are the standard errors of the means, and the dashed red line is for a difference of zero.

differences	# degree bins where the error bar does not cross zero	# frequency bins where the error bar does not cross zero
raw	12 of 14	10 of 16
normalized	10 of 14	14 of 16

Table 4: Number of degree and frequency bins, respectively, where the error bar does not cross zero for the comparison of the binned raw and normalized frequency differences $\Delta\nu = \nu_{\rm HMI.100430to0710.i.v0} - \nu_{\rm HMI.100430to0710.v7}$

In the first row of Table 4, we show the number of iplkm raw frequency difference bins for which the error bars did not cross zero and the total number of bins. We show that when the binning was done as a function of degree 86 % of the error bars did not cross zero and when the binning was done as a function of frequencies 63 % of the error bars did not cross zero. In the second row of this table, we show the similar statistics for the normalized iplkm frequency differences. For these differences the percentage of the degree bins for which the error bars did not include zero was 71 % for the degree bin and 88 % for the frequency bins. These four percentages are all large enough to indicate that at the level of one standard error of the mean, both the binned raw and binned normalized frequency differences for the iplkm case showed systematic differences from zero. In particular, the degree distribution of the bins whose error bars do not cross zero supports the idea that the most significant feature in the two left-hand panels of Figure 9 is the large dip that is centered on $l = 850$. Similarly, the frequency distribution of the bins whose error bars do not cross zero supports the idea that the most significant feature in the two right-hand panels of Figure 9 is the dip centered on the frequency of $2750\,\mu$Hz.

In Figure 10 we show both the raw and the normalized differences $w_{\rm HMI.100430to0710.i.v0} - w_{\rm HMI.100430to0710.v7}$ of the line widths both as functions of the spherical harmonic degree and of the frequency. As can be seen from the upper-left panel, aside from a few low-degree outliers the raw differences of the line widths are generally smaller than about $1\,\mu$Hz. The normalized differences of the line widths, $\Delta w/\sigma_{\Delta w}$, as shown in the bottom panels, do not exceed the $\pm 1\,\sigma$ level, apart from a few high-frequency outliers. In comparison with the lower panels of Figure 4, the lower panels of Figure 10 show that the use of interpolation in the leakage matrices resulted in smaller differences in the line widths than did the use of the non-zero B angle. Allowing for the difference in the sense of the subtractions in the two cases, the change in the iplkm widths would agree in sign with the positive differences that were shown in the lower panels of Figure 4.

Because the presence of the large outlying raw line width differences in both of the upper panels of Figure 10 obscured the presence of any possible systematic differences, we binned these raw line width differences as functions of both degree and frequency. The binned raw iplkm line widths differences are shown in the left-hand panel of Figure 11, and they are shown as a function of frequency in the right-hand panel. The left-hand panel shows a decrease above $l = 420$; the right-hand panel shows small random differences for frequencies below $2000\,\mu$Hz followed by a broad dip centered around $\nu = 3250\,\mu$Hz. The error bars in both panels are the standard errors of the mean values within each bin. In the left-hand panel we can see that, when the binning was done as a function of degree, 88 % of the error bars do not cross zero, while in the right-hand panel, when the binning was done as a function of frequency, 81 % of the error bars do not cross zero. These two percentages are large enough to indicate that at the level of one standard error of the mean, both sets of binned raw line width differences for the iplkm case showed systematic differences from zero. Keeping in mind the change in sign of the iplkm comparisons relative to the Bang comparisons, the systematic decreases seen in both panels of Figure 11 actually correspond to systematic increases in the binned line widths in the sense of the Bang line width comparison. Comparing the absolute

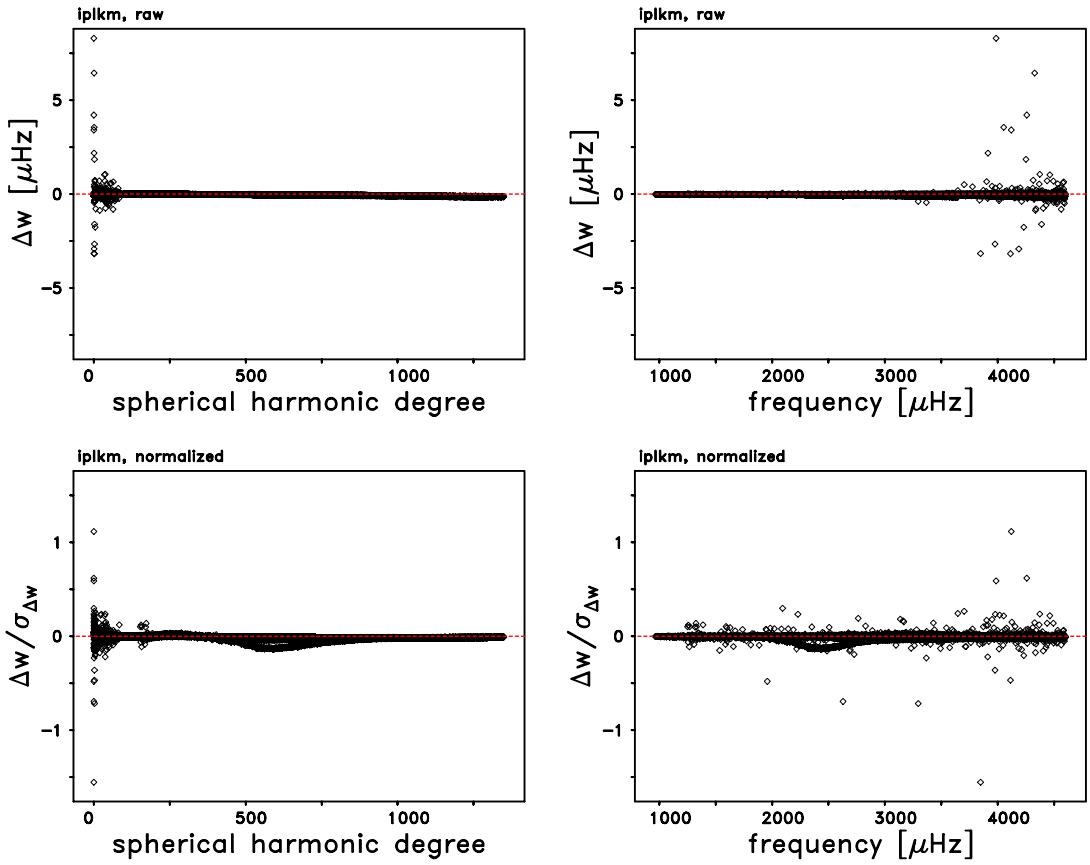

Figure 10: (Upper-left panel) Line width differences $\Delta w = w_{\mathrm{HMI.100430to0710.i.v0}} - w_{\mathrm{HMI.100430to0710.v7}}$ as functions of the spherical harmonic degree for the ridges $n = 0$ through $n = 30$. The dashed red line is for a difference of zero. (Upper-right panel) Same as upper-left panel, but for the line width differences Δw as functions of the frequency. (Bottom-left panel) Same as upper-left panel, but for the normalized line width differences. The normalization was carried out by dividing the raw line width differences, Δw, as shown in the upper left-hand panel, by the formal error, $\sigma_{\Delta w}$, of each difference. (Bottom-right panel) Same as bottom-left panel, but for the normalized line width differences as functions of the frequency.

value of the largest difference in the left-hand panel of Figure 11 with the absolute value of the largest difference in the corresponding panel of Figure 5, we can see that the iplkm line width changes were roughly 2.5 times larger than the corresponding Bang line width changes

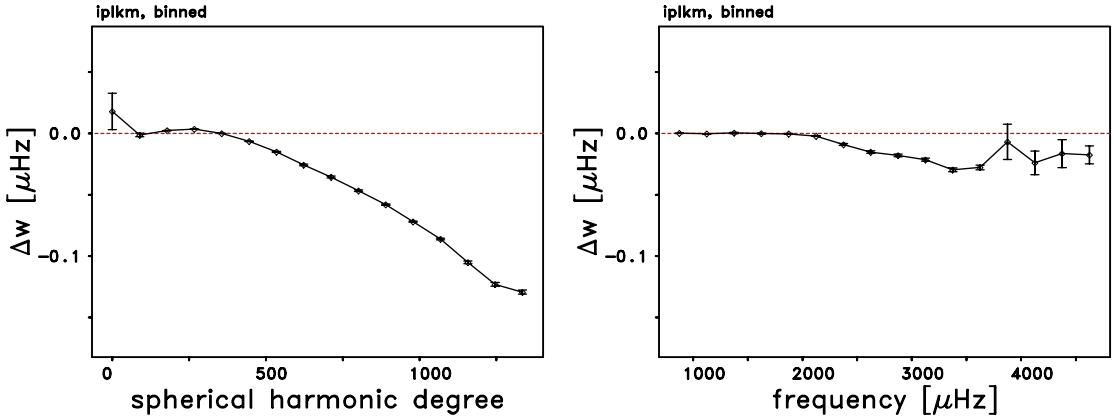

Figure 11: (Left panel) Binned line width differences $\Delta w = w_{\mathrm{HMI.100430to0710.i.v0}} - w_{\mathrm{HMI.100430to0710.v7}}$ as functions of the spherical harmonic degree for the ridges $n = 0$ through $n = 30$. The dashed red line is for a difference of zero. (Right panel) Same as left-hand panel, but for the binned line width differences Δw as functions of the frequency.

In Figure 12 we show both the raw and the normalized differences $B_{\rm HMI.100430to0710.i.v0} - B_{\rm HMI.100430to0710.v7}$ of the line asymmetries as functions of the spherical harmonic degree. Appreciable raw differences of the line asymmetries only occur for $l < 250$. Apart from two outliers, the normalized differences of the line asymmetries, $\Delta B/\sigma_{\Delta B}$, are in the range $\pm 1\,\sigma$.

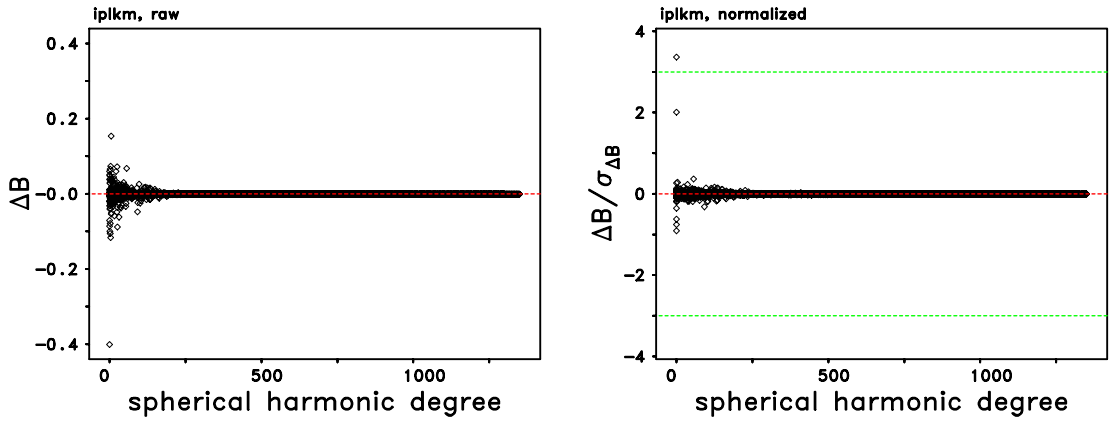

Figure 12: (Left panel) Line asymmetry differences $\Delta B = B_{\rm HMI.100430to0710.i.v0} - B_{\rm HMI.100430to0710.v7}$ as functions of the spherical harmonic degree for the ridges $n = 0$ through $n = 30$. The dashed red line is for a difference of zero. (Right panel) Same as left panel, but for the normalized line asymmetry differences. The normalization was carried out by dividing the raw line asymmetry differences, ΔB, as shown in the left-hand panel, by the formal error, $\sigma_{\Delta B}$, of each difference. The dashed green line shows the $+3\,\sigma$ value.

We show the binned raw asymmetry differences for the iplkm case as functions of degree and frequency in Figure 13. Both panels of this figure show that, apart from a single bin located at both low degrees and low frequencies, the iplkm raw asymmetry changes were small and random.

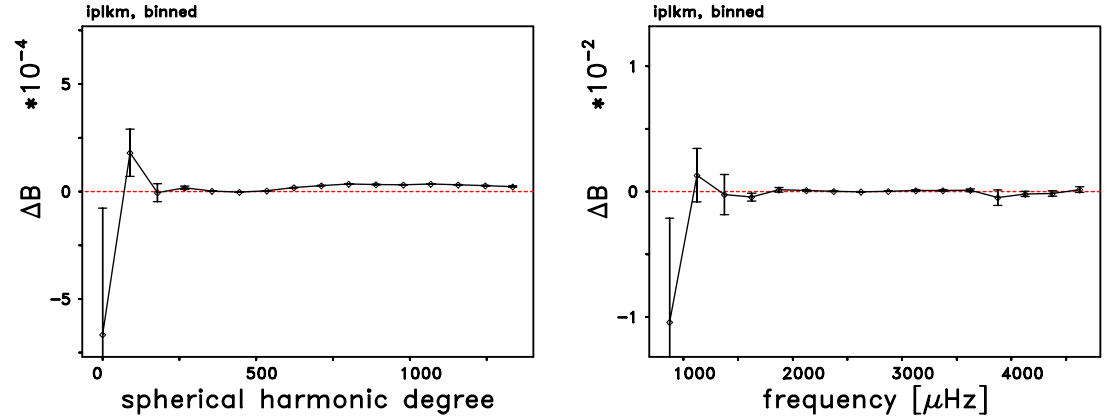

Figure 13: (Left panel) Binned line asymmetry differences $\Delta B = B_{\rm HMI.100430to0710.i.v0} - B_{\rm HMI.100430to0710.v7}$ as functions of the spherical harmonic degree for the ridges $n = 0$ through $n = 30$. The dashed red line is for a difference of zero. (Right panel) Same as left-hand panel, but for the binned line asymmetry differences ΔB as functions of the frequency.

C) Comparison of B-angle and Interpolation effects on Scaled Relative Frequency Differences

Shortly after we had completed sections A) and B) above, Dr. Jesper Schou sent us a reference to a paper by Basu, *et al.* (2003), in which she and her co-authors computed scaled relative frequency

differences for several different tables of model frequencies that had been computed using both the GONG and MDI observations at three different levels of solar activity. Specifically, these authors generated four different frequency tables at each of the different levels of activity. One of these four frequency tables came from the application of the GONG data processing pipeline, which they referred to as the "AZ" pipeline, to a time series of GONG observations. The second frequency table came from the application of the AZ pipeline to a simultaneous set of MDI observations. The third table came from the application of the Stanford pipeline, which these authors referred to as the "CA" pipeline to the set of MDI observations, while the fourth table came from the application of the CA pipeline to the set of GONG observations. Since these authors presented figures that illustrated the scaled relative frequency differences for the four frequency tables that were generated from a time interval of relative low activity and they also presented comparisons of the results of structural inversions using these four frequency tables, we decided to compute one set of scaled relative frequency differences for the Bang case and a second set for the iplkm case.

Basu, *et al.* (2003) defined the scaled relative frequency differences as $Q_{n,l}\Delta\nu_{n,l}/\nu_{n,l}$, where $Q_{n,l}$ is the ratio of the mode inertia $I_{n,l}$ of a mode with degree l and order n to that of a mode of degree zero with the same frequency. Even though they found that their average relative errors were typically less than 1×10^{-5}, which they pointed out was substantially smaller than the formal errors in the differences, they also pointed out that some of their frequency differences showed "... a systematic behavior that might nonetheless influence the inversion results."

In order to be able to better compare the effects of both the use of a non-zero B-angle and of interpolation in the leakage matrices, we employed a table of $Q_{n,l}$ values that extended up to $l = 1350$ and converted our two sets of raw frequency differences into two sets of scaled relative frequency differences. As soon as we had finished generating both sets of scaled relative frequency differences, we computed the overall averages of these differences, and we computed the standard deviations about these averages. We show the number of differences for both comparisons in the second column of Table 5. We show both average differences in the third column of this table, and we show both standard deviations in the fourth column of this table. In the fifth column, we show the T-statistic for both comparisons, and in the sixth column we show the probability that each set of differences was a random occurrence. At the same significance level of 2.5 percent for the null hypothesis that we used earlier for the raw and normalized frequency differences, both of these probabilities suggest that the two sets of overall scaled relative frequency differences were not statistically significant from zero."

comparison	$n_{\rm d}$	ave	std	t	p
Bang	7329	$+3.66 \times 10^{-7}$	1.96×10^{-5}	1.600	0.110
iplkm	7327	-1.50×10^{-7}	1.89×10^{-5}	0.677	0.498

Table 5: Statistics of the differences in the scaled relative frequency differences for the comparisons listed in the first column. In the second column the number of differences is listed. The average and the standard deviation of the difference is listed in the third and fourth column, respectively. In the fifth column the value of the t-statistic is listed, while in the last column the probability is given that the difference is random.

Even though the overall average values of both the Bang and iplkm comparisons were not statistically different from zero, we wanted to explore whether either set of frequency differences contain any systematic differences as functions of either the degree or the frequency of the modes that were being compared, so we plotted both sets of the scaled relative differences as functions of both variables, and we also binned both sets of differences as functions of both degree and

frequency. We show the differences that resulted from the Bang comparison in Figure 14. In the left-hand panel of Figure 14 we show the dependence of these scaled relative frequency differences as a function of degree, while in the right-hand panel, we show them as a function of frequency. Because the vertical scale of both panels in this figure are dominated by two groups of low-degree modes, one at frequencies below about 1500 μHz and the other above 3800 μHz, it is impossible to tell if there might be any systematic differences in either panel. Hence, we also binned the Bang frequency differences as functions of both degree and frequency. We show both sets of binned scaled relative frequency differences in the two panels of Figure 15. The left-hand panel shows that the differences decrease monotonically with increasing degrees above $l = 200$, although all of the binned differences for degrees above $l = 300$ are less than 0.5×10^{-6}. In fact, only three of the 14 lower error bars cross zero in this panel. On the other hand, the right-hand panel of Figure 15 indicates that, for frequencies above 1500 μHz, the binned differences are all smaller than about 1×10^{-6}. So, from an examination of the two panels in Figure 15, the Bang comparison results in very small frequency differences that vary more systematically as a function of degree.

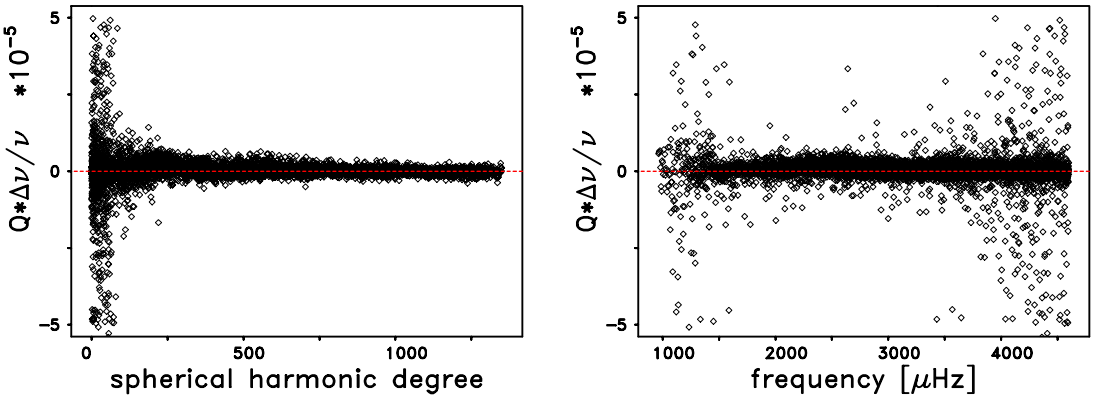

Figure 14: (Left panel) Scaled relative frequency differences $Q\,\Delta\nu/\nu$ as functions of the spherical harmonic degree for the ridges $n = 0$ through $n = 30$. Here, Q is the ratio of the mode inertia to that of a mode of degree 0 with the same frequency, and $\Delta\nu = \nu_{\rm HMI.100430to0710.v7} - \nu_{\rm HMI.100430to0710b-6.354.v0}$. The dashed red line is for a difference of zero. (Right panel) Same as left-hand panel, except that $Q\,\Delta\nu/\nu$ is plotted versus frequency.

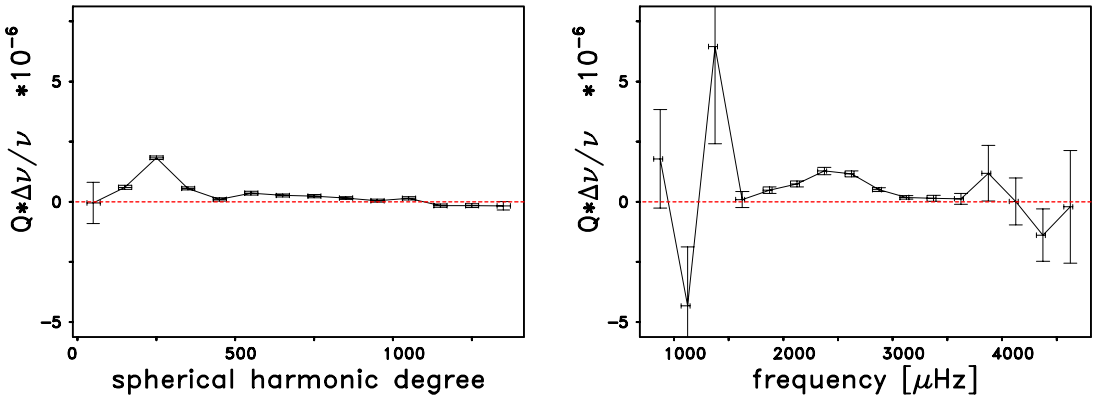

Figure 15: Same as Figure 14, except that the scaled relative Bang frequency differences $Q\,\Delta\nu/\nu$ have been binned using 100-degree and 250 μHz wide bins, respectively.

We also show the scaled relative frequency differences that resulted from the iplkm comparison in Figure 16. Again, these differences are shown as a function of degree in the left-hand panel, while they are shown as a function of frequency in the right-hand panel. As was the case in both panels of Figure 14, both panels of Figure 16 are dominated by a large scattering of outlying cases at low degrees and at both low and high frequencies, so that it is not possible to see any systematic effects in either panel. On the other hand, a quick comparison of Figures 14 and 16 illustrates that the use of the non- zero B-angle resulted in slightly larger frequency differences than did the use of interpolation. This difference in the size of the Bang and iplkm differences was also shown in the third column of Table 5. We show the binned scaled relative frequency differences for the iplkm case in the two panels of Figure 17. As was the case for the Bang comparison that was shown in Figure 15, the two panels of Figure 17 indicate that the frequency differences varied more systematically as a function of degree than they did as a function of frequency.

For degrees between $l = 500$ and $l = 1100$, the binned iplkm frequency differences show a parabolic behavior with the largest negative difference occurring for degrees around $l = 850$. Since, as we have already pointed out several times, the sense of the iplkm subtractions was opposite the sense of the Bang subtractions, after we mentally flip the signs of the differences shown in Figure 17, we see that the apparent parabolic dip in the binned scaled relative frequency differences was actually an upward bump.

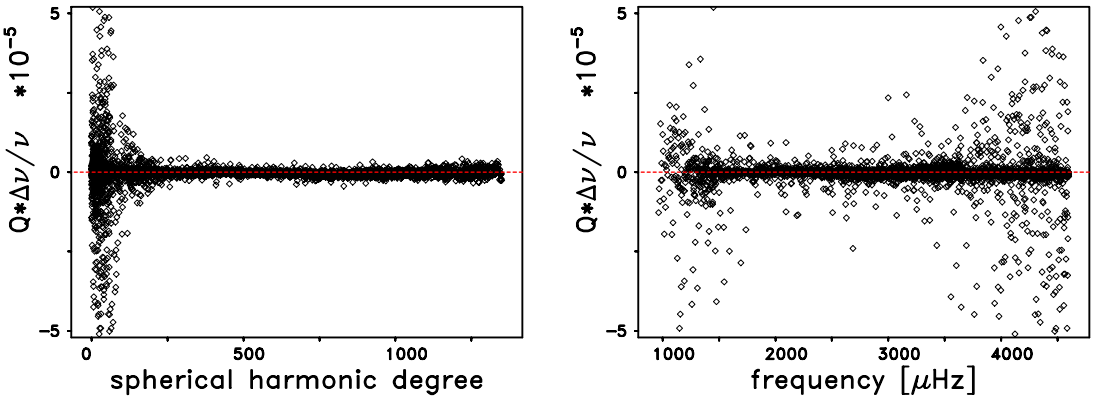

Figure 16: (Left panel) Scaled relative frequency differences $Q\,\Delta\nu/\nu$ as functions of the spherical harmonic degree for the ridges $n = 0$ through $n = 30$. Here, Q is the ratio of the mode inertia to that of a mode of degree 0 with the same frequency, and $\Delta\nu = \nu_{\rm HMI.100430to0710.i.v0} - \nu_{\rm HMI.100430to0710.v7}$. The dashed red line is for a difference of zero. (Right panel) Same as left-hand panel, except that $Q\,\Delta\nu/\nu$ is plotted versus frequency.

Before we compare our two sets of scaled relative frequency differences with the sets presented by Basu *et al.* (2003), it is important to provide more background on that paper. One of their pairs of time series came from an interval of low solar activity (which they defined as having an average value of the 10.7-cm coronal radio flux of 73 SFU, where 1 SFU = $10^{-22}\,{\rm Wm^{-2}Hz^{-1}}$), while the second pair came from an intermediate level of activity (which they defined as having an average 10.7-cm flux of 105 SFU), and the third pair came from a high level of activity (which they defined as having an average value of the 10.7-cm flux of 174 SFU). For each of the three different levels of solar activity, those authors generated four different frequency datasets for a total of 12 different frequency datasets. From the four frequency tables at a given level of activity, they computed a total of four different sets of frequency differences, which they referred to as: a) MDI(CA)-MDI(AZ), b) MDI(CA)-GONG(CA), c) GONG(AZ)-MDI(AZ), and d) GONG(AZ)-GONG(CA).

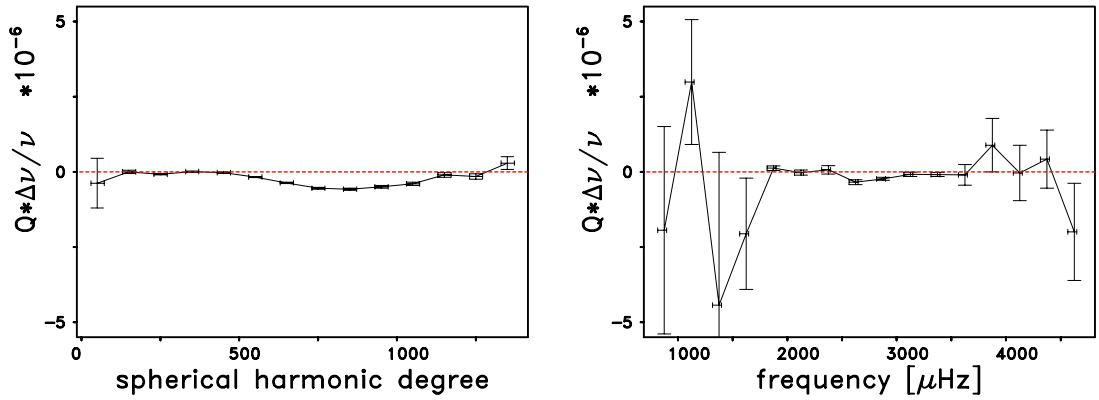

Figure 17: Same as Figure 16, except that the scaled relative iplkm frequency differences $Q\,\Delta\nu/\nu$ have been binned using 100-degree and 250 μHz wide bins, respectively.

The set of these frequency differences that we have found most closely matches our own Bang and iplkm frequency differences is case b) the MDI(CA)-GONG(CA) low-activity case. This set of frequency differences contained the smallest differences and the smallest amount of scatter. The low level of activity in case also closely matched the level of solar activity that existed during the time interval from which our frequencies were derived. For the 72-day time interval which began on April 30, 2010, the average 10.7-cm coronal flux was 75.4 SFU. The other three sets of low-activity frequency differences all included some differences that were considerably larger than any of our differences, and all of the other sets of differences showed much larger amounts of scatter. Furthermore, these authors did not publish their frequency differences from either the intermediate or high levels of activity, so we could not directly compare our results with any of those sets of differences.

The scaled relative frequency differences that are shown in the right-hand panels of both Figures 14 and 16 can be directly compared with the four different sets of similar quantities that were presented in Figure 2 of Basu *et al.* (2003). While the range of frequencies that we are analyzing is wider than the range of 1600 to 4400 μHz that they employed in their comparisons, over this common frequency range the differences that we are showing in the right-hand panel of Figure 14 look very similar in magnitude and in the amount of scatter to the differences shown in Figure 2(b) of Basu *et al.* (2003) for their MDI(CA)-GONG(CA) case. On the other hand, the differences in the right-hand panel of our Figure 16 look to be somewhat smaller than any of the four sets of differences that Basu *et al.* (2003) showed in their Figure 2.

Turning to the normalized frequency differences, $\Delta\nu/\sigma_{\Delta\nu}$, the normalized Bang frequency differences, that we showed in the lower right-hand panel of Figure 1 above look very similar to the normalized frequency differences that were presented in Figure 4(b) of Basu *et al.* (2003). Furthermore, the normalized iplkm frequency differences that we presented in the lower-right panel of Figure 8 above were generally smaller than the differences shown in Figure 4(b) of Basu *et al.* (2003).

Basu *et al.* (2003) also presented the 12 sound-speed perturbation profiles that they computed by inverting each of their 12 sets of frequencies. They found that the pair of profiles which agreed the most closely corresponded to their MDI(CA)-GONG(CA) low-activity case b). They showed these two profiles in their Figure 6(b). Since our Bang frequency differences that were shown in Figure 14 compared most closely with the Basu *et al.* (2003) MDI(CA)-GONG(CA) low-activity differences, and the two inverted profiles which they obtained from those two frequency tables were nearly indistinguishable, we expect that the inversions that will result from our HMI.100430to0710b-

6.354.v0 and HMI.100430to0710.v7 frequency tables will also be nearly indistinguishable. Also, since our iplkm frequency differences that we showed in Figure 16 were smaller than our Bang differences, we also expect that the inversion that will result from our HMI.100430to0710.i.v0 frequency table will likewise be indistinguishable from the inversion of our HMI.100430to0710.v7 table.

D) Conclusions

In addition to showing in Table 5 and in Figures 15 and 17 that both the Bang and iplkm changes in the leakage matrices resulted in very small scaled relative frequency changes, we showed in Tables 1 and 3 and in Figures 5 and 11 that the iplkm changes resulted in larger raw line width changes than did the Bang changes. On the other hand, we also showed in Figures 7 and 13 that the Bang changes resulted in more systematic changes in the asymmetries as a function of degree than did the iplkm changes.

Finally, the proof of our claims that both sets of the scaled relative frequency are small enough that they will not result in noticeable changes in the radial profile of the inverted sound speed will have to await actual structural inversions of all three of our frequency tables. On the other hand, it is very important to note that all three of our HMI MPTS frequency datasets cover a wider range of frequencies and a much wider range of degrees than do any of the datasets employed by Basu *et al.* (2003), so we might be surprised to find some differences in the results of the structural inversions of our three frequency tables.